Journal of Global Positioning Systems (*2021*)
Vol. 17, No. 2: 164-177
DOI: 10.5081/jgps.17.2.164

Research on the UWB High Precision Indoor Positioning Method with the Heterogeneous Information Constraints

Nan Guo[1]; Wei Jiang[2]; Jing Li[3]; Fei Liu[1*]; Jie Dong[3]
1 School of Geomatics and Urban Spatial Informatics, Beijing University of Civil Engineering and Architecture, Beijing 102616
2 State Grid Corporation of China, Beijing 100031
3 State Grid Siji Shenwang Location-Based Service (Beijing) Co., Ltd, Beijing 102209
* Corresponding author: Fei Liu, liufei1@bucea.edu.cn

Abstract: There are many obstacles in the UWB indoor positioning, such as installation location limitation of base stations, non-line-of-sight and so forward. In this paper, the high-precision indoor positioning model was discussed, and then the UWB indoor positioning method was given based on the heterogeneous data constraints, such as PDR, map and vision. Three indoor positioning models, the kinematic adaptive robust EKF UWB model based on the gain matrix, the UWB/PDR/Map coupled model, and the UWB/Vision fusion model were built and assessed, respectively. Afterward, the precision and the potential application scenarios of the three models were discussed via the practical tests. The test results showed that, with our method, the overall positioning accuracy reached around ±0.2 m under the conditions of the full or partial UWB signal coverage, available or interrupted line-of-sight, or undergoing other situational challenges such as the sparse texture and the continuous variation of the light strength.

Key words: Heterogeneous information; UWB; Robust EKF; Indoor location

1 Introduction

In spatial information science and engineering, the acquisition and processing of high-precision positioning information belong to the frontier research worldwide [1]. Many efforts have been made to consistently advance the techniques in this area, for example [2], the "Xihe" plan in China, the “Insight into the battlefield” and the “Next Generation 911 Project” in US, and the “Galileo Local Technology Plan” in Europe. With the completion of global coverage of the BDS (Beidou System) and other global satellite navigation systems, the real-time, all-weather operational condition, and global high precision PNT (Positioning, Navigation and Timing) are enabled to survey many outdoor applications [3,4].

With the indoor positioning and navigation techniques, even there are many options, such as WiFi [5], UWB (Ultra Wide Band) [6], RF (Radio Frequency) [7], and Bluetooth [8, 9], the meter-level positioning results may be easily to be achieved, however, developing the higher precision of indoor positioning techniques is still extremely challenging.

Specifically, the UWB positioning can reach the accuracy level of decimeters or even centimeters by measuring the transmission time, the angle, and the strength of electromagnetic wave signals between a positioning tag and a base station [10]. When UWB is used in positioning, its methods can be divided into RSSI (Received Signal Strength Indication), TDOA (Time Difference of Arrival), AOA(Angle-of-Arrival), TOA (Time of Arrival), etc. The positioning based on RSSI needs to be modeled according to the signal propagation fading to realize ranging. It can not reflect the advantages of UWB when applied to UWB [11]. AOA can overcome the influence of NLOS

Editor in charge: Dr. Xiaolin Meng

(Non Line of Sight) propagation to a certain extent and can locate with fewer sensors, but the cost is high due to the need to use antenna array and directional antenna angle measurement [12]. TOA can make full use of the advantages of high UWB time resolution, but the problem of clock synchronization at the transceiver must be solved first [13]. TDOA can overcome the problem of synchronization at the transceiver, but the synchronization between anchor nodes still needs to be considered [14].

However, due to the signal obstruction or reflection of variant structural objects and/or other solid features indoors, there may exist serious multipath effect, irregular LOS (Line of Sight) propagation, etc., which negatively affect the positioning accuracy, as well as the configuration of tags and base stations, pre-installation and measurement of the precise location of the base stations, etc., which restrict the positioning accuracy and even working area. Wymeersch [15] analyzed the characteristics of a large number of UWB signals in LOS and NLOS environments. Using SVM (Support Vector Machine, SVM) to identify the NLOS state and weaken the error can effectively eliminate the NLOS error and improve the ranging accuracy, but a large amount of data statistics is needed. Li [16] used Kalman filter to smooth the original ranging information and proposes a colored noise adaptive Kalman method to eliminate NLOS error. The simulation effect is obvious, but the amount of calculation is large. Meng [17] analyzed the geometric structure of the wall when the IR-UWB (Impulse Radio UWB) signal propagated through the wall, deduced the upper limit of the ranging error caused by the additional delay, and directly corrected the TOA ranging result by using the NLOS distance error information. This method requires more a priori knowledge and is difficult to be applied to the ranging elimination of moving targets.

Essentially, INS (Inertial navigation system) used in PDR (Pedestrian dead reckoning) algorithm uses accelerometers, and gyroscopes to obtain position, velocity, and attitude information and plays an important role in the field of navigation and location services. But its sensor technology and integration calculation principle restrict its popularization. A standalone INS system is difficult to satisfy the demand of the long-term navigation and positioning accuracy requirements [18]. As a streaming media technology, the video sensors have the capability of positioning and the acquisition of the environmental information, and the relative positioning accuracy may reach 0.1% to 2% of the working ranges. However, one find the use the visual method very challenging in environments such as sparse textures, too bright or too dark indoors [19, 20]. In this case, these sensors to assist UWB for fusion positioning can effectively make up for the shortcomings of each system. Building a hybrid positioning system can enhance the continuity and robustness of positioning in complex indoor environment. Renaudin [21] designed an optimal combined filter to fuse the arrival angle and arrival time difference of UWB signal with the acceleration, angular velocity and magnetic field intensity output by MEMS inertial system, so as to further suppress the UWB NLOS error. Zhang [22] used extended Kalman filter to fuse MEMS, UWB and barometer to form a position and heading estimation system, and obtained more reliable vertical positioning results. Nyqvist [23] presented a method for global pose estimation using INS, monocular vision, and UWB sensors, and showed the benefit of the suggested sensor combination. Qiao [24] used the position information output by monocular vision ORB (Oriented Fast and Rotated Brief)-SLAM (Simultaneous Localization and Mapping) and the positioning information calculated by UWB as measurement information, and used extended Kalman filter for data fusion to realize indoor positioning, which effectively overcomes the problem of unable positioning caused by monocular vision ORB-SLAM tracking failure, and effectively suppresses the influence of UWB NLOS error.

Our research has been targeting such problems mentioned above. This manuscript particularly discusses three different indoor positioning methods based on using UWB, PDR, and the vision sensors, and assesses the performance improvement with the proposed models. In the practical tests, the challenging environment were considered through the

reduction of the number of UWB base stations, varying the LOS obstruction, environmental texture and light strength through their influence on the indoor positioning accuracy. Afterward, the overall precision and potential application scenarios of the three methods were discussed based on the practical tests.

2 Extended Kalman filter

The classical Kalman filter is based on the linear system, that is, both the measurement model and the system model are linear systems. For discrete linear systems, the state equation can be described as:

$$\boldsymbol{x}_k = \boldsymbol{\Phi}_{k,k-1}\boldsymbol{x}_{k-1} + \boldsymbol{G}_{k-1}\boldsymbol{w}_{k-1} \tag{1}$$

where, $\boldsymbol{x}_k$ represents the state vector, $\boldsymbol{\Phi}_{k,k-1}$ represents the state transition matrix, $\boldsymbol{G}_{k-1}$ represents the system noise drive matrix and $\boldsymbol{w}_{k-1}$ represents the process noise vector. k is represented as an observation epoch.

Observation vectors and state vectors should simultaneously satisfy certain functional relationships. The observation equation of a discrete linear system can be expressed as:

$$\boldsymbol{z}_k = \boldsymbol{H}_k\boldsymbol{x}_k + \boldsymbol{v}_k \tag{2}$$

where, $\boldsymbol{z}_k$ represents the system observation vector, $\boldsymbol{H}_k$ represents the observation coefficient matrix and $\boldsymbol{v}_k$ represents the observed noise vector. For a classical Kalman filter, the process and observation noise vectors should conform to the following normal distributions:

$$\begin{cases} \boldsymbol{w}_k \sim N(\boldsymbol{0}, \boldsymbol{Q}_k) \\ \boldsymbol{v}_k \sim N(\boldsymbol{0}, \boldsymbol{R}_k) \end{cases} \tag{3}$$

where $\boldsymbol{Q}_k$ and $\boldsymbol{R}_k$ are the positive definite covariance matrices of process noise and observation noise vectors, respectively [25].

Kalman filter is a recursive estimation process based on system state and noisy observation sequence, which usually includes time update process and measurement update process.

The time update process is as follows[26]:

$$\begin{cases} \hat{\boldsymbol{x}}_k^- = \boldsymbol{\Phi}_{k,k-1}\hat{\boldsymbol{x}}_{k-1}^+ \\ \boldsymbol{P}_k^- = \boldsymbol{\Phi}_{k,k-1}\boldsymbol{P}_{k-1}^+\boldsymbol{\Phi}_{k,k-1}^T + \boldsymbol{G}_{k,k-1}\boldsymbol{Q}_{k-1}\boldsymbol{G}_{k-1}^T \end{cases} \tag{4}$$

where the symbols "^", "-" and "+" represent the estimated, predicted, and filtered value, respectively. $\hat{\boldsymbol{x}}_k^-$ and $\boldsymbol{P}_k^-$ are the state prediction and its covariance matrix at t_k, $\hat{\boldsymbol{x}}_{k-1}^+$ and $\boldsymbol{P}_{k-1}^+$ are the state estimate and its covariance matrix at t_{k-1}, respectively.

The measurement updating process is as follows:

$$\begin{cases} \boldsymbol{K}_k = \boldsymbol{P}_k^-\boldsymbol{H}_k^T(\boldsymbol{H}_k\boldsymbol{P}_k^-\boldsymbol{H}_k^T + \boldsymbol{R}_k)^{-1} \\ \hat{\boldsymbol{x}}_k^+ = \hat{\boldsymbol{x}}_k^- + \boldsymbol{K}_k(\boldsymbol{z}_k - \boldsymbol{H}_k\hat{\boldsymbol{x}}_k^-) \\ \boldsymbol{P}_k^+ = (\boldsymbol{I} - \boldsymbol{K}_k\boldsymbol{H}_k)\boldsymbol{P}_k^- \end{cases} \tag{5}$$

where, $\boldsymbol{K}_k$ is the filter gain matrix, which is calculated with the minimum state variance as the constraint condition.

The predicted residual is as follows:

$$\boldsymbol{V}_k = \boldsymbol{z}_k - \boldsymbol{H}_k\hat{\boldsymbol{x}}_k^- = \boldsymbol{z}_k - \hat{\boldsymbol{z}}_k \tag{6}$$

Linear system is only an ideal system. In practical applications, system state models or observation models mostly contain non-linear characteristics. The EKF (Extended Kalman filter) is one of the most commonly used estimation method for nonlinear filtering problems in scientific and engineering applications. The system model is as follows:

$$\boldsymbol{x}_k = \boldsymbol{f}_{k-1}(\boldsymbol{x}_{k-1}, \boldsymbol{w}_{k-1}) \tag{7}$$

along with the observation model:

$$\boldsymbol{z}_k = \boldsymbol{h}_k(\boldsymbol{x}_k, \boldsymbol{v}_k) \tag{8}$$

The noise matrix of EKF non-linear system still satisfies the requirement of Formula (3). Before time update, the system needs to linearize the state equation by first order Taylor series expansion to get the state transition matrix and noise drive matrix, which can then be solved as KF.

$$\begin{cases} \boldsymbol{\Phi}_{k,k-1} = \left.\dfrac{\partial \boldsymbol{f}_{k-1}}{\partial \boldsymbol{x}}\right|_{\hat{\boldsymbol{x}}_{k-1}^+} \\ \boldsymbol{G}_{k-1} = \left.\dfrac{\partial \boldsymbol{f}_{k-1}}{\partial \boldsymbol{w}}\right|_{\hat{\boldsymbol{x}}_{k-1}^+} \end{cases} \tag{9}$$

At the same time, the observation equation needs to be linearized to obtain the observation coefficient matrix before updating the measurements.

$$\boldsymbol{H}_k = \left.\frac{\partial \boldsymbol{h}_k}{\partial \boldsymbol{x}}\right|_{\hat{\boldsymbol{x}}_k^-} \tag{10}$$

After the state equation and the observation equation are discretized, the state can be updated by the methods of equations (4) and (5).

3 The UWB indoor positioning with the heterogeneous information constraints

3.1 The robust EKF using UWB

Under the consideration that the motion process involves position, velocity and acceleration information, this paper proposes a 9-dimensional state vector UWB dynamic positioning model based on EKF model. The state vectors are as follows:

$$\boldsymbol{x}_k = [\Delta \boldsymbol{x} \quad \Delta \dot{\boldsymbol{x}} \quad \Delta \ddot{\boldsymbol{x}} \quad \Delta \boldsymbol{y} \quad \Delta \dot{\boldsymbol{y}} \quad \Delta \ddot{\boldsymbol{y}} \quad \Delta \boldsymbol{z} \quad \Delta \dot{\boldsymbol{z}} \quad \Delta \ddot{\boldsymbol{z}}] \tag{11}$$

where $\Delta \boldsymbol{u}, \Delta \dot{\boldsymbol{u}}, \Delta \ddot{\boldsymbol{u}}$ ($\boldsymbol{u}$ = x, y, z) represent the position, velocity and acceleration errors in the $\boldsymbol{u}$ direction, respectively. The accelerations can be considered as a first-order Markov process [27]. Both of the process noise vector and the observation noise vector are considered to the zero-mean white noise processes. The state coefficient matrix can be obtained from the motion model:

$$\boldsymbol{\Phi}_k = \begin{bmatrix} \boldsymbol{\Phi}_{x,k} & 0 & 0 \\ 0 & \boldsymbol{\Phi}_{y,k} & 0 \\ 0 & 0 & \boldsymbol{\Phi}_{z,k} \end{bmatrix} \tag{12}$$

with

$$\boldsymbol{\Phi}_{u,k} = \begin{bmatrix} 1 & T & \dfrac{T^2}{2} \\ 0 & 1 & T \\ 0 & 0 & 1 \end{bmatrix} \tag{13}$$

where T represents the time interval. The observable is the range from a UWB mobile station to each base station, and the spatial geometric distance P is:

$$P_i = \sqrt{\left(x_i - x_a\right)^2 + \left(y_i - y_a\right)^2 + \left(z_i - z_a\right)^2} \tag{14}$$

where, $\left(x_a, y_{a,} z_a\right)$ is the location coordinates of UWB mobile station, $\left(x_i, y_{i,} z_i\right)$ is the coordinates of the i-th base station. After linearizing the above formula, the approximate coordinates $\left(x_{a0}, y_{a0,} z_{a0}\right)$ of the mobile station tag are brought in as the initial value to obtain the observation equation:

$$P_i' = P_{a0}' - \begin{bmatrix} l_a & m_a & n_a \end{bmatrix} \begin{bmatrix} \Delta x \\ \Delta y \\ \Delta z \end{bmatrix} \tag{15}$$

with $P_{a0}' = \sqrt{\left(x_i - x_{a0}\right)^2 + \left(y_i - y_{a0}\right)^2 + \left(z_i - z_{a0}\right)^2}$,

$l_a = \dfrac{x_i - x_{a0}}{P_{a0}'}$, $m_a = \dfrac{y_i - y_{a0}}{P_{a0}'}$ and $n_a = \dfrac{z_i - z_{a0}}{P_{a0}'}$.

Therefore, the observation matrix is:

$$H = [l_a \quad 0 \quad 0 \quad m_a \quad 0 \quad 0 \quad n_a \quad 0 \quad 0] \tag{16}$$

But, when the observations contain gross errors, the state estimation will be biased so that the influence of gross errors in measurements cannot be ignored. In this paper we construct a robust EKF gain matrix that can restrict the effect of the gross errors on the state estimation as [28]:

$$\tilde{\boldsymbol{K}}_{ij} = \begin{cases} \bar{\boldsymbol{K}}_{ij} & s_j \le c_0 \\ \bar{\boldsymbol{K}}_{ij} \times \dfrac{c_0}{s_j} \times \left[\dfrac{c_1 - s_j}{c_1 - c_0}\right]^2 & c_0 < s_j \le c_1 \\ 0 & s_j > c_1 \end{cases} \tag{17}$$

where, c_0 and c_1 are robust parameters. c_0 is 2.5-3.5, c_1 is 3.5-4.5[28].

$$s_j = \left|V_{k,j}\right| \Big/ \sqrt{r_j \sigma_j} \tag{18}$$

where i represents the i-th component in the state vector, and j represents the j-th component in the observation vector, $V_{k,j}$, r_j and σ_j represents the

prediction residual(Equation 6), redundancy index [29] and a-priori standard deviation of the *j*-th observation, respectively. At epoch *k*, the redundancy index r_j of the *j*-th observation is generally defined by:

$$r_i(k) = (\boldsymbol{Q}_{V_y}(k)\boldsymbol{W}_y(k))_i \tag{19}$$

where $\boldsymbol{Q}_{V_y}(k)$ is the covariance matrix of the residual vector and $\boldsymbol{W}_y(k)$ is the weighting matrix of the observation vector under the assumption of a diagonal matrix. The covariance matrix of the residual vector for the observation vector is:

$$\boldsymbol{Q}_{V_y}(k) = \boldsymbol{H}_k \boldsymbol{P}_k^{-} \boldsymbol{H}_k^T + \boldsymbol{R}_k \tag{20}$$

3.2 The UWB/PDR/Map fusion

The range and its accuracy from the UWB indoor positioning technique are restricted by the number of the base stations and their distribution. The positioning performance degrades if the UWB signals become weak. Sometime, the UWB system may even become unavailable. Hence, the integration of UWB, PDR (pedestrian dead reckoning) and Map is introduced. The corresponding EKF is designed to include the position errors dN and dE, the moving distance error ds and the heading error $d\theta$ in its state vector [30]:

$$\boldsymbol{x}_k = [dN \quad dE \quad ds \quad d\theta]^T \tag{21}$$

According to the PDR motion model, the state transition matrix should be:

$$\boldsymbol{\Phi}_k = \begin{bmatrix} 1 & 0 & \cos\theta_k & -s_k \sin\phi_k \\ 0 & 1 & \sin\phi_k & s_k \cos\theta_k \\ 0 & 0 & 1 & 0 \\ 0 & 0 & 0 & 1 \end{bmatrix} \tag{22}$$

When the position of the UWB system is updated, the position difference between the UWB and PDR system is taken as the observation as follows:

$$\boldsymbol{z}_k = [\Delta N \ \Delta E]^T = [N_{k,u} - N_{k,p} \ E_{k,u} - E_{k,p}] \tag{23}$$

Then the observation matrix is：

$$H_k = \begin{bmatrix} 1 & 0 & 0 & 0 \\ 0 & 1 & 0 & 0 \end{bmatrix} \tag{24}$$

where ΔN and ΔE are the north and east position differences between the two positioning systems, $N_{k,u}$ and $E_{k,u}$ are the north and east UWB positions, $N_{k,p}$ and $E_{k,p}$ are the north and east positions calculated according to the PDR algorithm at time *k*.

When the output of the UWB position is not updated, the differences between the system prediction coordinates and the PDR observation coordinates are taken as the observations, and the rest remains unchanged, and the PDR position is recursively corrected.

The position errors obtained through filtering are used to update the predicted positions at the current time. So, the final position is updated as follows [31]:

$$\begin{cases} N_{p,k}^{+} = N_{p,k} + dN \\ E_{p,k}^{+} = E_{p,k} + dE \end{cases} \tag{25}$$

In order to suppress the divergence of the heading estimate obtained from the INS, we match the position with the indoor map based on the UWB positioning result, and virtually design 16 possible equally spaced directions around this position, i.e., every other 22.5 degrees. The direction of the center of the section is adopted as the moving direction of a pedestrian. Relative to the heading angle of the inertial navigation system, the center direction of the nearest interval is used as the heading. If the difference between the heading from the inertial navigation and the nearest map direction is less than 5 degrees, the heading angle of the inertial navigation is used as the current heading [30].

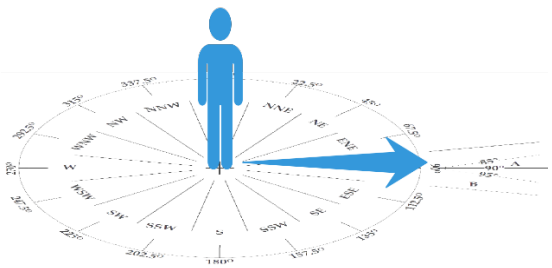

Fig.1 Heading angle calculating strategy

3.3 UWB/Vision Fusion

Visual sensors can be used not only for positioning during emergency rescues such as urban fires and earthquakes, but also for acquiring the environment information to compensate the UWB's insufficient environmental perception. However, the visual positioning technique is affected by a single texture, light and dark changes, etc., which are prone to positioning failure. Moreover, monocular vision SLAM (simultaneous localization and mapping) suffers from scale drift and axial blur. For this reason, upon the UWB EKF positioning model and the monocular vision SLAM model [32], a UWB/vision fusion model is proposed here for indoor positioning under the consideration of the visual scale factors and heading deviations [33] with the following state vector at t_k :

$$\boldsymbol{x}_k = [\boldsymbol{X}_k \quad \boldsymbol{Y}_k \quad \boldsymbol{v}_k \quad \boldsymbol{\theta}_k \quad \boldsymbol{s}_k \quad \boldsymbol{\varphi}_k]^T \tag{26}$$

where, $\boldsymbol{X}_k$ and $\boldsymbol{Y}_k$ represent plane coordinates, $\boldsymbol{v}_k$ represents pedestrian speed, $\boldsymbol{\theta}_k$ represents the angle of movement direction, $\boldsymbol{s}_k$ represents the ambiguity of the scale, and $\boldsymbol{\phi}_k$ represents the deflection angle between the plane coordinates calculated by vision and the plane coordinates calculated by UWB.

According to the error equation of vision and UWB, the corresponding state equation is:

$$\boldsymbol{x}_{k+1} = \begin{bmatrix} 1 & 0 & sin\theta & 0 & 0 & 0 \\ 0 & 1 & cos\theta & 0 & 0 & 0 \\ 0 & 0 & 1 & 0 & 0 & 0 \\ 0 & 0 & 0 & 1 & 0 & 0 \\ 0 & 0 & 0 & 0 & 1 & 0 \\ 0 & 0 & 0 & 0 & 0 & 1 \end{bmatrix} \boldsymbol{x}_k + \begin{bmatrix} \boldsymbol{w}_x \\ \boldsymbol{w}_y \\ \boldsymbol{w}_v \\ \boldsymbol{w}_\theta \\ \boldsymbol{w}_s \\ 0 \end{bmatrix} \tag{27}$$

Where $\boldsymbol{w}_x$ and $\boldsymbol{w}_y$ respectively represent the plane position error, $\boldsymbol{w}_v$, $\boldsymbol{w}_\theta$ and $\boldsymbol{w}_s$ represent the speed error, heading angle error and visual scale factor error respectively. If the visually measured position, heading, and the UWB measured position are taken as the observations, the UWB/vision observation equations are as given below:

$$\begin{bmatrix} \boldsymbol{X}_{uwb} \\ \boldsymbol{Y}_{uwb} \end{bmatrix} = \begin{bmatrix} 1 & 0 & 0 & 0 & 0 & 0 \\ 0 & 1 & 0 & 0 & 0 & 0 \end{bmatrix} \boldsymbol{X} + \boldsymbol{e}_{uwb} \tag{28}$$

$$\begin{bmatrix} \boldsymbol{X}_{vision} \\ \boldsymbol{Y}_{vision} \end{bmatrix} = \begin{bmatrix} cos\phi & -sin\phi & 0 & 0 & \boldsymbol{X}_{vision} & 0 \\ sin\phi & cos\phi & 0 & 0 & \boldsymbol{Y}_{vision} & 0 \end{bmatrix} \boldsymbol{X} + \boldsymbol{e}_{vision} \tag{29}$$

wherein $\boldsymbol{X}_{vision}$ and $\boldsymbol{Y}_{vision}$ are the position coordinates derived from the vision sensor, $\boldsymbol{X}_{uwb}$ and $\boldsymbol{Y}_{uwb}$ are the position derived by UWB, $\boldsymbol{e}_{vision}$ is the vision position measurement noise vector, and $\boldsymbol{e}_{uwb}$ is the UWB position measurement noise vector.

4 The Multisource indoor positioning fusion framework

In order to overcome the obstacles that are oftern faced in UWB indoor positioning technique, the robust EKF UWB positioning model based on adaptive gain matrix, the UWB/PDR/map integrated positioning model and the UWB/vision integrated positioning model shown in Figure 2 have been proposed, repectively, and used to improve the UWB indoor positioning technique inclusive of reducing the number of the UWB base stations and the impact of the indoor non-line-of-sight, as well as the indoor environment perception, frequent changes in light and localization of areas with sparse texture.

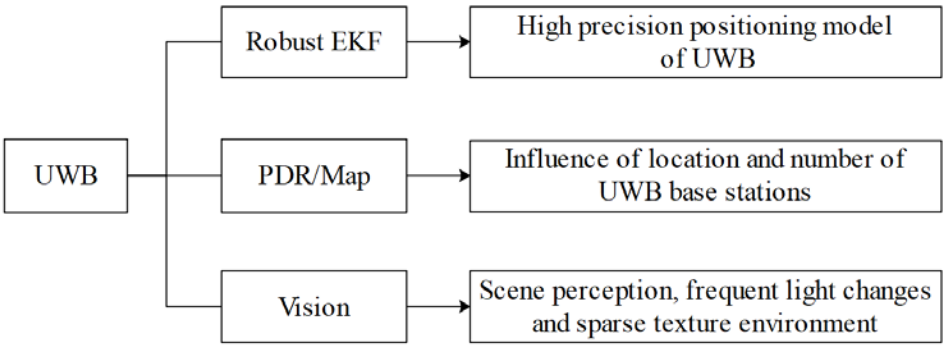

Fig. 2 Heterogeneous information fusion positioning framework

5 Results and their analysis

5.1 UWB robust EKF positioning results analysis

The UWB equipment used in this paper is shown in Figure 3, which can be set as base station or mobile station by command, and automatically change the working mode. The equipment mainly consists of UWB chip, 4G communication module and a package structure. When it is set as a mobile station, it can measure the distance between it and each base station, and transmit the distance information to the upper computer system through 4G module. Its performance is shown in the Table 1.

Fig.3 UWB anchor and tag two-in-one device

Table 1 Performance of UWB anchor and tag two-in-one device

Performance	Parameter
Size	12.5*9.5*2cm
Receiving sensitivity	-118dBm
Ranging accuracy	≤12cm
Positioning accuracy	≤30cm
Line-of-sight ranging distance	Max 800m
Positioning sampling rate	1Hz

The experimental scene is on the laboratory floor (as shown in Figure 4), and the corridor is about 65m long and 3M wide. Several positioning base stations (red triangle in the figure in Figure 5) are set in the classroom and corridor, and their point coordinates are determined by the total station to establish a relative coordinate system. The experimenter walked at a constant speed (from left to right) along the established route with UWB mobile station, as shown in Figure 5, the trajectory results of different algorithms are showed.

Fig.4 Experimental environment

Figure 6 shows the positioning errors resulted from least squares, EKF and the robust EKF method in this paper. It can be seen that the three positioning trajectories well agree with the real trajectory. The 2D root mean square error was ±1.18m from the least square method. The same root mean square error was ±0.28m from the EKF and ±0.13mfrom the proposed method, from which 94% of the point error was better than ±0.50m, and 6% of the point error between ±0.50m-±1.00m.

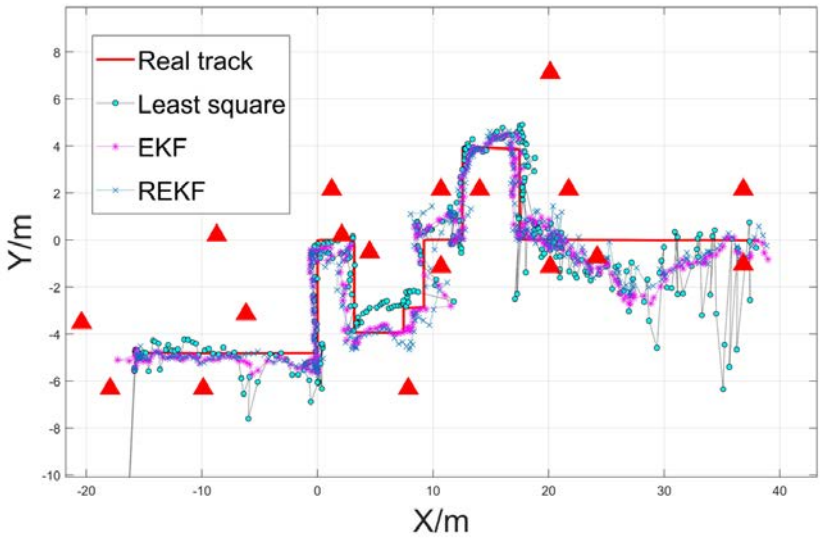

Fig.5 Positioning result track

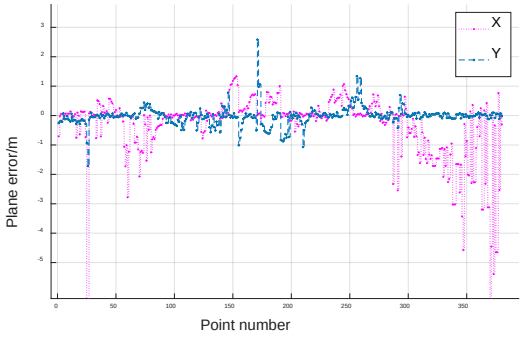

(a) Least square positioning error

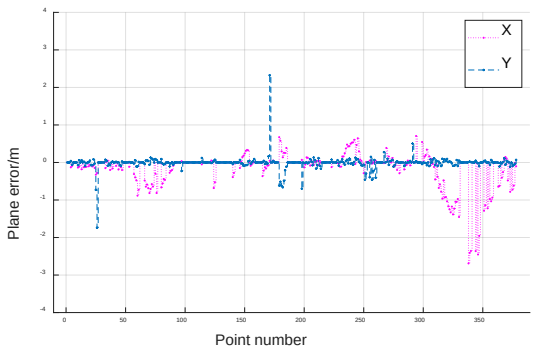

(b) EKF positioning error

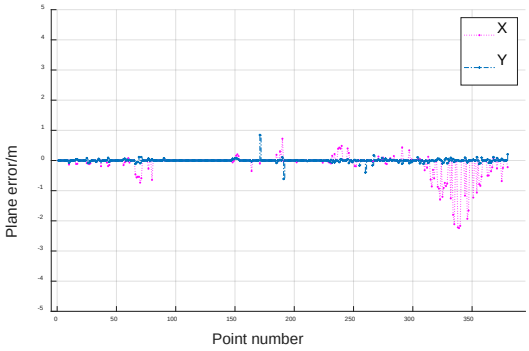

(c) Robust EKF positioning error

Fig.6 Positioning trajectory and errors

5.2 UWB/PDR/Map Fusion

5.2.1 UWB with full signal coverage

In this experiment, a MEMS IMU named MPU9250 is used, which has 9-axis accelerpmeter, gyroscope and magnetometer producted by InvenSense Company(Sunnyvale, CA,USA). Some of its performance parameters are as Table 2. During the experiment, UWB and IMU were bound to the instep of the experimenter, as shown in Figure 7.

Table2. MPU9250 partial parameters

Performance	Parameter
Operating Voltage Supply	2.4V to 3.6V
Gyro Full Scale Range	±250 ±500 ±1000 ±2000 °/s
Gyro Rate Noise	0.01 dps/Hz
Gyro Sensitivity Scale Factor	TYP 32.8 LBS/(°/s)
Gyro Rate Noise Spectral Density	0.01d°/s/√ Hz
Accel Sensitivity Scale Factor	4,096 LSB/g
Accel Noise Power Spectral Density	300μg/√ Hz
Accel Full Scale Range	±2 ±4 ±8 ±16 g
Accel Sensitivity	±4800 LSB/g

Fig.7 Equipment placement

For the best performance, an ideal working environment was introduced for conducting our experiments, in which the UWB signal covered the entire positioning area. 12 UWB base stations cover part of the corridor and a laboratory, as shown in the red triangle in the Figure 8. The experiment takes the north as the Y axis and the East as the X axis.

So, as in Figure 8, the positioning trajectories from the UWB, unconstrained PDR, and map-constrained PDR could be obtained. The UWB positioning result was basically coicided with the actual trajectory and had the root mean square errors: ±0.13m in the X direction and ±0.16m in the Y direction. However, due to the low positioning frequency (1 Hz) of UWB and the long time interval of updating the position information, it is easy to cause the problem of positioning discontinuity at the corner. The PDR positioning track has ranged from indoor to outdoor and had the root mean square errors about ±1.55m in the X direction and about ±2.06m in the Y direction. The PDR positioning method on map constraints escaped from the above situation, and its solution was in good agreement with the real trajectory, but early or late turns did happen. The corresponding root mean square errors were about ±0.25m in the X direction and about ±0.40m in the Y direction. By using this method, the estimated trajectory was basically consistent with the actual one, and further the integration with the PDR data, the positioning rate was improved, and the problem of discontinuous positioning at the corner is avoided. The solution had the root mean square errors of about ±0.15m in the X direction and about ±0.18m in the Y direction.

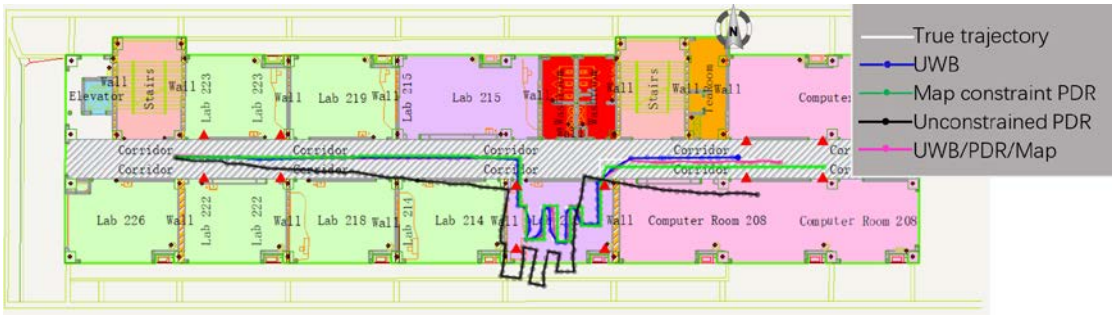

Fig.8 UWB location results with the full signal coverage

5.2.2 UWB partial coverage scenarios

In order to study the UWB performance with the partial singal coverage, two signal lock-out scenarios were simulated. Figure 9(a) shows the scenario where the UWB signal lost lock three times, and the time interval of each loss of lock was 5 seconds. Figure 9(b) shows the scenario where UWB signals were only available at both ends of the corridor and indoors.

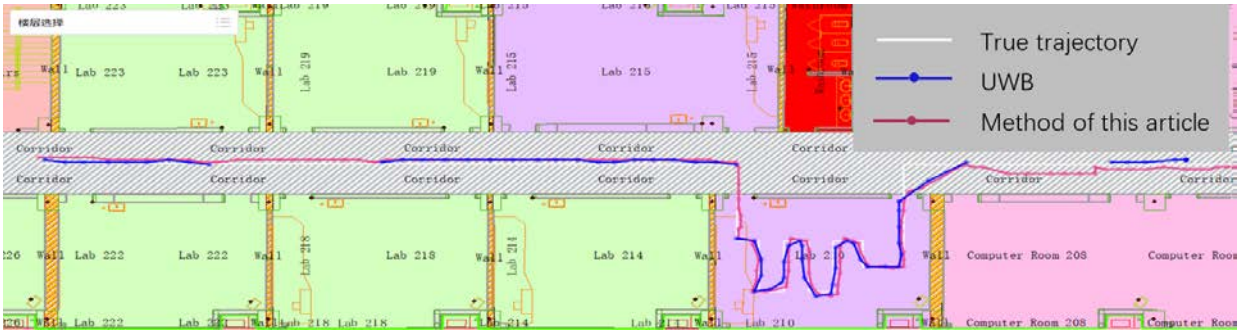

(a) Locate the track when the signal is out of lock 3 times

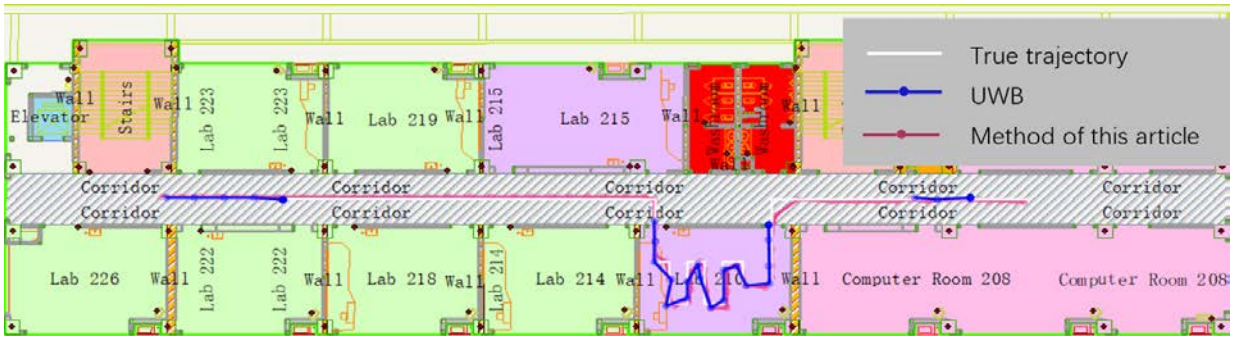

(b) Locate the trajectory when most UWB signals in the corridor lose lock

Fig.9 Positioning results when UWB signal is partially covered

A summary is given here. The blue line in Figure 9 represents the UWB positioning track, with the missing parts where the UWB signals were not available. As can be seen, with the UWB signals, high-precision positioning can still be achieved. In the uncovered area, even if there was no UWB positioning result, the positioning was still achieved with the aid of PDR data. However, the positioning accuracy was quickly droped down as only the map-constrained PDR positioning result was made available in 1-2 seconds after the UWB signal lost lock. The quantitative analysis of the results in Figures 9(a) and 9(b) gave the root mean square errors of about ±0.11m in the X direction and about ±0.20m in the Y direction from the former. From the latter, the root mean square error of X direction was about ±0.19m and the Y direction was about ±0.38m, which means that, when indoors, the base station equipment was located on the ground and affected by non-line-of-sight, the positioning accuracy was degraded. In addition, the availability of the UWB positioning solution was low, which resulted in an increased trajectory inconsistency at short-distance turns, further with increasing of the positioning errors.

5.3 UWB/visual fusion

5.3.1 Experiments in light change environment

The camera used in the experiment is the Guardian camera (Figure 10) purchased by Taobao, and its performance parameters are shown in the Table 3. The experimental scenario is shown in the Figure11. We placed four UWB base stations in four corners of the laboratory. The experimenter held the camera and UWB bound together and circled clockwise three times along the established route.

Fig.10 Guardian camera

Fig.11 Experimental scene

Table 3.Performance of the Guardian camera

Performance	Parameter
Frame rate(FPS)	10
Fx(pixels)	3637.74
Fy(pixels)	3658.25
Resolution(pixels)	1920 * 1080
Brightness mode	AUTO

When a camera faces the window, the brightness of its images will decrease, especially when it is rotating. Conversely, when it faces the opposite direction, the brightness will increase. Frequent changes in light brightness may cause SLAM positioning to fail. Figure 12 shows the positioning results from UWB, vision and their fusion. The blue circles and red triangles in the figure represent the location points from the UWB and the combination of UWB and vision, respectively, while the blue line represents the actual trajectory. Besides, Figure 12(b) presents the visual location result while Figure 12(c) plots the positioning errors of the UWB/vision fusion solution. From Figure 12(a), most of the UWB positioning results were consistent with the designed route, but there were also a certain number of the positioning points with large differences from the actual route, for example, the points at the left bottom corner, on the top and at some other positions. The 2D root mean square error was ±0.32m. From Figure 12(b), firstly, some of the results accurately described the walking trajectory; secondly,the monocular positioning method only delivers the relative positioning information; thirdly, a few of the factors, such as sparse texture, brightness changes and in-situ turns etc., caused positioning failures many times. Finally, in the process, although SLAM's loopback detection and back-end optimization improved the positioning results, there were still some large errors at the upper right corner. In the fusion positioning results, almost all the red dots were distributed on both sides of the actual route, which indicated that the integrated solution was more accurate than the solution using the UWB technique alone and gave the 2D root mean square error of ±0.18m. In addition, the fusion algorithm also functions to limit the visual positioning errors (Figure 12(b)) and solve the problem due to the scale blur.

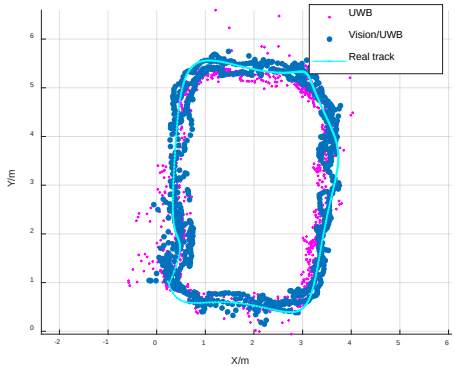

(a) UWB/visual fusion

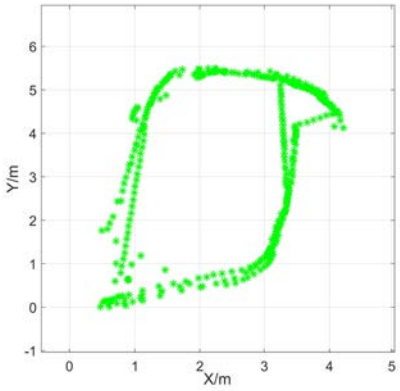

(b) Visual positioning

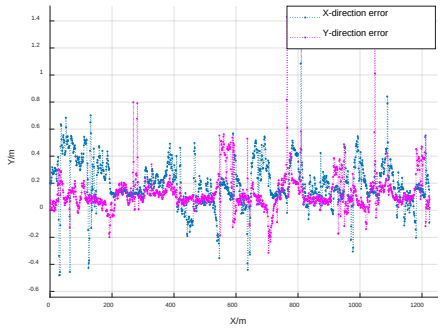

(c) Fusion positioning errors

Fig.12 Location results of UWB / vision fusion in light changing environment

5.3.2 Experiments in sparse texture environment

Figure 13 shows the positioning results in the sparsely textured corridors and classrooms with white walls. In Figure 13(a), the red and blue curves present the UWB and the UWB/vision integrated positioning results, respectively, while the green curve presents the real trajectory. The integrated positioning results were in good agreement with the actual trajectory and had the root mean square error of ±0.17m. In the integration, UWB provides the absolute positioning information and also functions as the initial vision positioning parameters. In case the vision positioning fails, the positioning can be resumed on the spot, thereby the continuous positioning is ensured. Figure 13(c) plots the positioning errors, in which the blue line is for UWB, and the red line for the UWB/vision fusion. From our analysis, about 53% of the points from the integrated solution were at an accuracy level of ±0.1 meters, about 22% at an accuracy of ±0.1-±0.2 meters, 25% at an accuracy of ±0.2-±0.3 meters, and 10% at an accuracy of ±0.3-±0.4 meters.

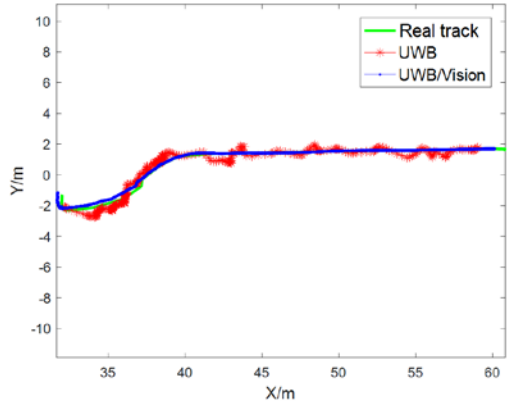

(a) UWB/visual fusion positioning results

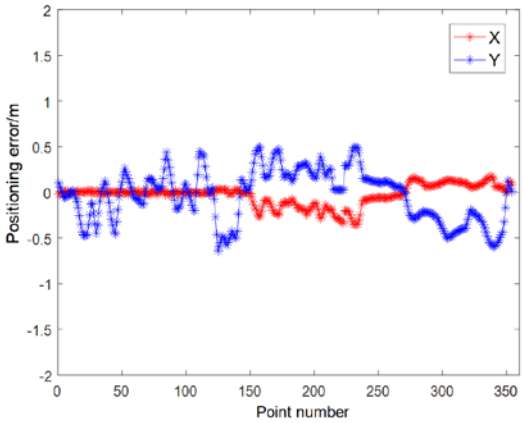

(b) UWB positioning residual

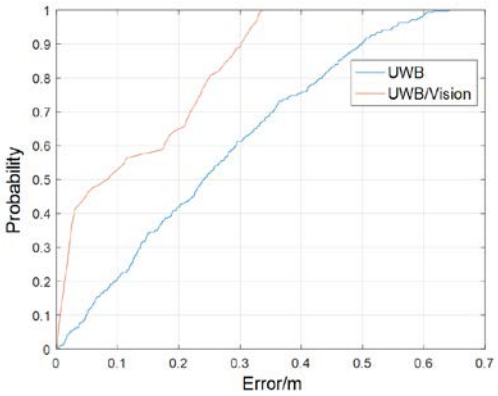

(c) Residual distribution curve

Fig. 13 Results from the UWB/vision fusion in sparse texture environment

6 Conclusions

To have aimed at the problems in the UWB indoor positioning, whose performance has been restricted by the location and number of available base stations, indoor non-line-of-sight and the inability to perceive the indoor environment in real time, this paper proposed a positioning approach based on heterogeneous information constraints such as UWB, PDR and vision. The UWB positioning model based on robust EKF can adjust the gain matrix according to the predicted residuals to reduce or eliminate the influence of gross errors on the state vector. The error in 2D planar positioning was about ±0.13m. Compared with the least squares and EKF algorithms, the positioning accuracy was increased by 88.98% and 53.57%, respectively. Apparently, UWB provides the absolute spatial reference for the PDR positioning and suppresses the divergence of the PDR positioning. At the same time, the use of the PDR technique in our experiments increased the positioning availability of the UWB technique, complementarily solved the positioning problem caused by poor UWB signal coverage or fully obstructed areas, and helped with indoor maps to suppress the PDR heading divergence and positioning divergence. The fusion positioning model based on UWB/vision nicely solved the problems of the scale errors in monocular vision SLAM, frequently required re-initialization due to environmental factors (resulting in discontinuous positioning), and the challenges due to sparse textures or frequent lighting changes in indoor

environments, and achieved a positioning accuracy of ±0.2m.

Although the integrated positioning strategy based on multi-source heterogeneous information has made great progress, it is still facing certain difficulty to satisfy the requirements of indoor and outdoor high-precision seamless positioning in emergency rescues such as urban fires and earthquakes. Therefore, the multi-sensor fusion that integrates positioning and scene perception, and wearable or simply assembled devices, when one conducts the positioning in complex environments, is still our next focus.

References

[1] LIU, Jingnan; GUO, Wenfei; GUO, Chi; et al (2020): Rethinking ubiquitous mapping in the intelligentage[J] . Acta Geodaeticaet Cartographica Sinica, 2020, 49(4):403-414.

[2] DENG, Zhongliang (2016): Status and development of navigation and location services[J]. Satellite Applocation, 2016, 50(2):43-47.

[3] YANG, Yuanxi; XU, Yangyin; LI, Jinlong; et al (2018): Progress and performance evaluation of BeiDou global navigation satellite system: Data analysis based on BDS-3 demonstration system[J]. Science China Earth Sciences, 2018, 61(5):614-624.

[4] JIANG, Weiping (2017): Challenges and opportunities of GNSS reference station network[J]. Acta Geodaetica et Cartographica Sinica, 2017, 46(10): 1379-1388.

[5] CHEN, Zhenghua; ZOU, Han; JIANG, Hao; et al (2015): Fusion of WiFi, smartphone sensors and landmarks using the Kalman filter for indoor localization [J]. Sensors, 2015, 15(1):715-732.

[6] XU, Liyuan (2019): Research on UWB-based relative localization algorithms in blind envrionment. Beijing:University of Science and Technology Beijing, 2019.

[7] STELLA, M.; RUSSO, M.; BEGUSIC, D.; et al (2012): RF localization in indoor environment[J]. Radioengineering, 2012, 21(2):557-567.

[8] CHEN, Ruizhi (2017): Mobile thinking engine leads intelligent location service[J]. Journal of Navigation and Positioning, 2017, 5(1):1-3.

[9] KRIZ, P; MALY, F and KOZEL, T (2016): Improving indoor localization using bluetooth low energy beacons[J]. Mobile Information Systems,2016,(2016-4-19), 2016, 2016(pt.2):1-11.

[10] SHI, Guowei and MING, Ying (2016): Survey of indoor positioning systems based on ultra-wideband (UWB) technology[C]. Wireless Communications, Networking and Applications. Springer. 2016: 1269-78.

[11] WANG, Chuanyang (2020): Study on UWB Positioning Method and Configuration Optimization [D]. China University of Mining and Technology.

[12] ZHANG, Hao; LIU Xing; Gulliver T A; et al (2013): AOA Estimation for UWB Positioning Using a Mono-station Antenna Array [J]. Journal of Electronics & Information Technology, 2013, 35(08):2024-2028.

[13] WANG, Changqiang; XU, Aigong; SUI, xin (2017):An indoor dynamic positioning method of UWB TW-TOA[J]. Science of Surveying and Mapping, 2017, v.42; No.234(12):151-156.

[14] KREISER D; MARTYNENKO D; KLYMENKO O; et al (2015): Simple and efficient localization method for IR-UWB systems based on two-way ranging[C]. 2015 IEEE MTT-S International Conference on Microwaves for Intelligent Mobility (ICMIM), 2015, pp. 1-4.

[15] WYMEERSCH H (2012): A Machine Learning Approach to Ranging Error Mitigation for UWB Localization[J]. IEEE Transactions on Communications, 2012, 60(6):1719-1728.

[16] LI Qiyue; WU Zhong; LI Jie; et al (2015): NLOS error elimination algorithm based on Improved Kalman filter [J]. Journal of Electronic Measurement and Instrumentation, 2015, 29(10):1513-1519.

[17] MENG Jing; ZHANG Qinyu; ZHANG Naitong; et al (2011): Modeling the distance error and performance analysis in IR-UWB positioning

system[J]. Journal on Communications, 2011, 32(06):10-16.

[18] ZHENG L; ZHOU W; TANG W; et al(2016): A 3D indoor positioning system based on low-cost MEMS sensors [J]. Simulation Modelling Practice and Theory, 2016:45-56.

[19] LIANG, J Z, CORSO, N, TURNER, E; et al (2013): Image based localization in indoor environments[C]// Computing for Geospatial Research and Application (COM.Geo), 2013 Fourth International Conference on. IEEE, 2013.

[20] FRAUNDORFER, F and SCARAMUZZA, D (2012): Visual Odometry : Part II: Matching, Robustness, Optimization, and Applications[J]. IEEE Robotics & Automation Magazine, 2012, 19(2):78-90.

[21] RENAUDIN, V; MERMINOD, B; KASSER, M (2008): Optimal data fusion for pedestrian navigation based on UWB and MEMS[C]. 2008 IEEE/ION Position, Location and Navigation Symposium, 2008,1(3):753-761.

[22] ZHANG, M; VYDHYANATHAN, A; YOUNG, A; et al(2012): Robust height tracking by proper accounting of nonlinearities in an integrated UWB/MEMS-based-IMU/baro system[C]. Position Location and Navigation Symposium(PLANS), 2012 IEEE/ION,2012:414-421.

[23] NYQVIST, H E; SKOGLUND, M A; HENDEBY, G; et al (2015): Pose Estimation Using Monocular Vision and Inertial Sensors Aided with Ultra Wide Band[C]// 2015 International Conference on Indoor Positioning and Indoor Navigation (IPIN). IEEE, 2015.

[24] QIAO, Z; XU, A; SUI, X; et al (2018): An integrated indoor positioning method using ORB-SLAM/UWB[J]. Navig. Positioning 2018, 6, 29-34.

[25] WANG, Jianguo (2008): Test Statistics in Kalman Filtering[J]. Journal of Global Positioning Systems, 2008, 7(1):81-90.

[26] HAN, Houzeng (2017): Research on the Key Models of INS aided BDS/GPS High Precision Kinematic Positioning [D]. China University of Mining and Technology.

[27] HAN, Houzeng; WANG, Jian; LIU Fei, et al (2019): An emergency seamless positioning technique based on ad hoc UWB Networking Using Robust EKF[J]. Sensors, 2019, 19(14).

[28] YU, Xuexiang and LU, Weicai (2000): Robust Kalman filtering model for dynamic data processing of GPS monitoring networks[J]. Journal of China University of Mining & Technology, 2000, 29(6): 553-557.

[29] WANG, Jianguo. (2009): Reliability Analysis in Kalman Filteirng[J]. Journal of Global Positioning Systems, 2009, 8(1):101-111.

[30] LIU, Fei; WANG, Jian; ZHANG, Jixian; et al (2019): An indoor localization method for pedestrians base on combined UWB/PDR/Floor Map[J]. Sensors, 2019, 19(11): 2578.

[31] LIU, Chunyan (2015): Study on the pedestrian indoor positioning algorithms based on WIFI and inertial technology[D]. Jiangsu:China University of Mining and Technology, 2015.

[32] MUR-ARTAL, R; TARDOS, J D (2017): ORB-SLAM2: An open-source SLAM system for monocular, Stereo, and RGB-D Cameras[J]. IEEE Transactions on Robotics, 2017, 1-8.

[33] LIU, Fei; ZHANG, Jixian; WANG, Jian; et al (2020): An UWB/Vision fusion scheme for determining pedestrians' indoor location[J]. Sensors, 2020, 20(4):1139.